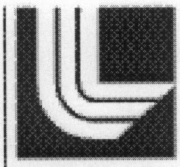

LAWRENCE
LIVERMORE
NATIONAL
LABORATORY

UCRL-JC-155163

Core Temperature and Density Profiles from Multispectral Imaging of ICF Plasmas

J. A. Koch, T. W. Barbee, Jr., S. Dalhed, S. Haan, N. Izumi, R. W. Lee, L. Welser, D. L. McCrorey, R. C. Mancini, F. Marshall, D. Meyerhoffer, C. Sangster, V. Smalyuk, J. Soures, L. Klein

August 26, 2003

2003 Third International Conference on Inertial Fusion Sciences and Applications, Monterey, CA
September 7-12, 2003

WO18.1

CORE TEMPERATURE AND DENSITY PROFILES FROM MULTISPECTRAL IMAGING OF ICF PLASMAS

J. A. Koch, T. W. Barbee, Jr., S. Dalhed, S. Haan, N. Izumi, R. W. Lee
University of California, Lawrence Livermore National Laboratory, Livermore CA, USA
email koch1@llnl.gov

L. Welser, D. L. McCrorey, R. C. Mancini
Department of Physics, University of Nevada, Reno NV, USA

F. Marshall, D. Meyerhoffer, C. Sangster, V. Smalyuk, J. Soures
Laboratory for Laser Energetics, University of Rochester, Rochester NY, USA

L. Klein
Department of Physics and Astronomy, Howard University, Washington DC, USA

We have developed a multiple monochromatic x-ray imaging diagnostic using an array of pinholes coupled to a multilayer Bragg mirror, and we have used this diagnostic to obtain unique multispectral imaging data of inertial-confinement fusion implosion plasmas. Argon dopants in the fuel allow emission images to be obtained in the Ar He-b and Ly-b spectral regions, and these images provide data on core temperature and density profiles. We have analyzed these data to obtain quasi-three-dimensional maps of electron temperature and scaled electron density within the core for several cases of drive symmetry, and we observed a two-lobed structure evolving for increasingly prolate-asymmetric drive. This structure is invisible in broad-band x-ray images. Future work will concentrate on hydrodynamics simulations for comparison with the data.

I. INTRODUCTION

In inertial confinement fusion (ICF) experiments, high-power pulsed laser beams are used to directly or indirectly ablate the outer surface of a spherical capsule containing hydrogen-isotope fuel [1]. The rocket effect drives the capsule to implode to a nearly isobaric compressed state, with maximum temperature and local-minimum density occurring at the center of the plasma. The final temperature and density profiles are determined by many factors, including laser drive symmetry, target symmetry, mixing of shell material into the fuel, and heat transport by electron and radiation conduction. Many of these factors have been investigated theoretically and experimentally [1].

X-ray imaging and spectroscopy have long been utilized as diagnostics of ICF plasmas, but indirect measurements of electron temperature (T_e) and electron density (N_e) profiles have only recently been obtained using these techniques [2]. In these experiments, traces of argon were added to the fuel for spectroscopic diagnosis, and monochromatic x-ray images [3] at photon energies corresponding to Ar He-β and Ar Ly-β were obtained along with x-ray spectra. A genetic algorithm-based numerical search through parameter space was then used to find the T_e and N_e profiles which best fit the imaging and spectroscopic data. Because single images are used, this technique cannot provide reconstructed profiles for either T_e or N_e without reliance on spatially-integrated x-ray spectra. Furthermore, spherical symmetry was assumed in the reconstruction process, eliminating the possibility of investigating T_e and N_e profiles in non-ideal implosions. The reconstructed profiles were also sensitive to distortion and astigmatism in x-ray imaging optics, and very bright individual images were required because no averaging could be performed.

We have developed a technique which allows direct measurement of T_e profiles and which is free from the limitations described above. We have used multiple-pinhole monochromatic imaging together with sophisticated data analysis to obtain monochromatic image *ratios* from Ar

He-β and Ar Ly-β energy bands. This technique, together with a generalized Abel inversion analysis, has provided direct quasi-three-dimensional (3D) reconstructions of T_e profiles, and as a corollary has allowed scaled N_e profiles to be obtained simultaneously. The results provide the first quasi-3D measurements of T_e and N_e profiles in ICF plasmas, and illuminate the hydrodynamics of asymmetrically-driven implosions.

II. EXPERIMENTS AND RESULTS

In our experiments, we used 30 500-joule, 1-ns-duration drive beams of the Omega Laser [4] to irradiate the inside surface of a 2.5-mm-long, 1.6-mm-diameter Au hohlraum (Fig. 1). The resulting x-ray drive imploded a 440-μm inner-diameter capsule containing 50 atm. of deuterium and 0.1 atm. of argon. The shell wall was 35 μm plastic, and the inner 3 μm was doped with Ti at 1.6% by weight to provide a spectroscopic diagnostic of shell conditions by absorption of core continuum emission [5].

We viewed the implosion from two nearly orthogonal directions near the midplane of the hohlraum, using identical multiple-monochromatic x-ray imaging (MMI) instruments. The MMI consists of the following major elements: an array of 1280 5-μm-diameter pinholes in a 25-μm-thick Ta substrate, placed at a distance of 16 mm from the target; a WB_4C multilayer Bragg mirror with an interplanar spacing of 1.51 nm, placed 82 mm from the target; and a time-integrated charge injection device (CID) x-ray detector placed 143 mm from the target. Each pinhole projects an image onto the CID, and the Bragg reflection restricts the spectral content of the image based on the bandpass of the mirror and on the instrument geometry. A similar instrument was previously used for implosion imaging in other experiments [6]. The detector was filtered with 600 μm of Be, and the length and dispersion of the mirror provided a spectral range of approximately 3300 to 5800 eV with a spectral resolution of approximately E/DE ~ 200. Typical data is shown in Fig. 1.

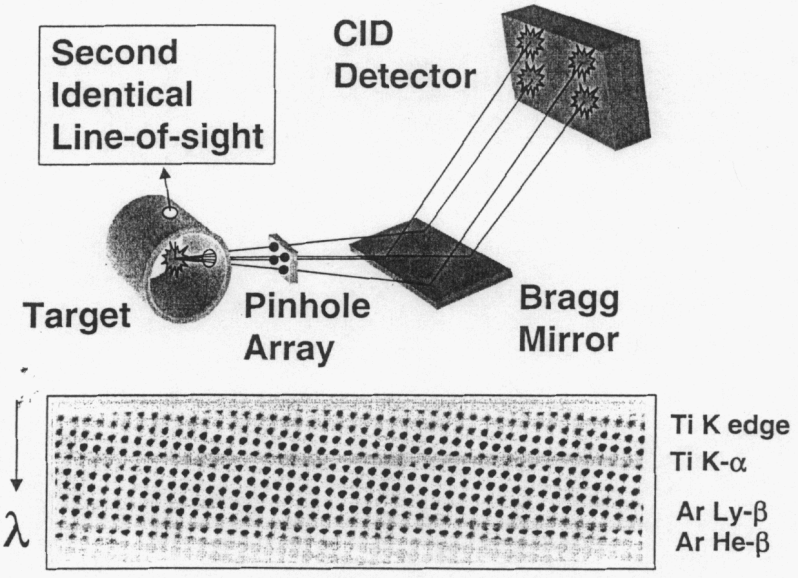

Figure 1: Sketch of the experimental geometry. The pinhole array is mounted on the target, and projects images onto an x-ray detector after reflection off a Bragg mirror, which restricts the spectral content of each image and introduces dispersion along the vertical axis of the detector. Two identical diagnostics were fielded, with typical data as shown.

Individual pinhole images were added numerically in order to improve signal-to-noise ratio and to decouple spatial resolution from spectral resolution. We first Fourier-transformed the complete CID image and fit the result to a synthetic pinhole function with the symmetry properties of the pinhole array used in the experiments (a square array projected at an arbitrary angle with respect to the detector and with arbitrary rotational orientation), in order to determine the centroid positions of the individual pinhole images in the detector plane. Using the centroid information, portions of many (typically 15-20) individual pinhole images could be

numerically added to generate a summed image within a specified spectral range, which was generally narrower than the spectral range of an individual pinhole image. Spectrally-dependent corrections due to filter transmission, CID sensitivity and quantum efficiency, and mirror reflectivity were then applied to the relative image intensities, and continuum images from the spectral region between the He-β and Ly-β lines were subtracted from He-β and Ly-β line-emission images. The results were relatively-calibrated, narrow-band images due to He-β and Ly-β emission only, averaged over dozens of individual pinhole images (see Fig. 2), with an estimated spatial resolution of 10 μm.

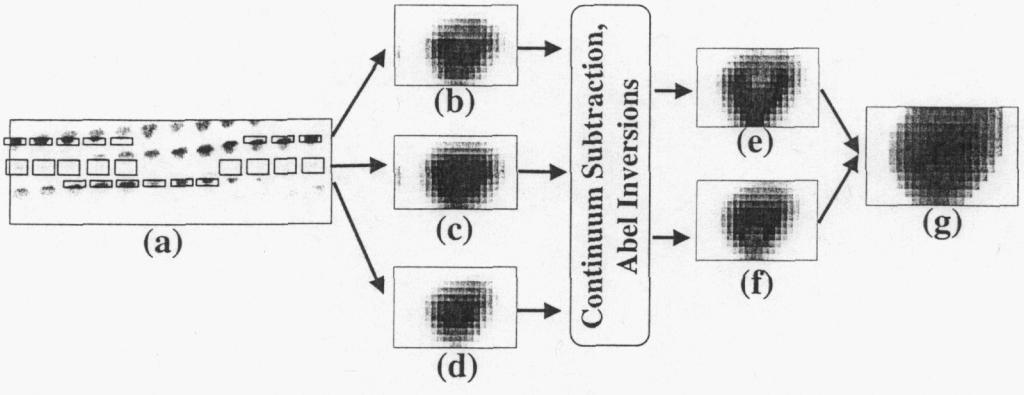

Figure 2: Data processing steps. Fractions of each image in the raw data (a) are added numerically to obtain narrow-band images with high signal-to-noise ratio in the He-β (b), continuum (c), and Ly-β (d) bands. Continuum images are subtracted from line images, and the resulting difference images, (e) and (f), are masked to show only regions where the contrast ratio is greater than 5%. The difference images are then Abel-inverted row-by-row to obtain emissivity maps, (g) and (h). The Ly-β map is divided by the He-β map, the spectral modeling is used to convert this ratio map into a local T_e map (i). The scale for all individual images is 100 μm square at the source.

We next Abel-inverted [7] the image intensity maps row-by-row to obtain radial emissivity maps relative to the peak image intensity of each row. In this step, we averaged the left- and right-sides of the image intensity profiles relative to the peak of each row. This process assumes that the plasma has rotational symmetry about a line parallel to the hohlraum axis (vertical in all images) in any plane perpendicular to the hohlraum axis; spherical or pure cylindrical symmetry need not be assumed. This assumption was checked by comparison between the two orthogonal viewing directions in Fig. 1, and the Abel-inverted emissivity profiles for each energy band (He-β and Ly-β) as functions of local radius r and longitudinal position z were obtained (Fig. 2). This process preserves the asymmetry of the original images, and in this sense is a quasi-3D reconstruction.

Dividing the Ly-β emissivity map by the He-β emissivity map results in a map of local line emission ratio in a plane containing the hohlraum axis, and this ratio map was transformed to a local T_e using an atomic kinetics code [8]. The line emissivities are well-fit by a functional form $\exp(f(T_e) + g(T_e)\ln(N_e))$, where $f(T_e)$ and $g(T_e)$ are 5th-order polynomials. The polynomials $g(T_e)$ for Ly-β and He-β are not identical, and therefore the emissivity ratio is not strictly independent of N_e, but the residual dependence of the inferred T_e upon N_e is weak. We used the time-averaged, space-averaged Stark line width of the He-β line (obtained from the same data) to infer an electron density of $N_e \approx 1\text{x}10^{24}$ cm^{-3}, and used this density to infer the temperature profiles. Assumptions of different densities primarily change the temperature scale but do not significantly change the shape of the temperature profile. Finally, the emissivity maps can be combined with the T_e maps to allow semi-quantitative N_e profiles to be extracted separately. Scaled densities cannot be obtained directly because the functions $g(T_e)$ depend

upon local temperature and because the data are not absolutely calibrated, but the general features of the density maps can be identified unambiguously.

T_e maps and profiles from several experiments are shown in Fig. 3. In Figs. 3(a) -3(b), the laser drive symmetry was tuned to produce a nearly spherical implosion; in Fig. 3(d) the laser drive symmetry was tuned 30 μm towards the equator to produce a mild prolate asymmetry, while in Fig. 3(e) the laser drive symmetry was tuned 60 μm towards the equator to produce a stronger prolate asymmetry. The corresponding scaled N_e maps and profiles are shown in Fig. 4. All maps in Figs. 3 and 4 are masked to display only those pixels which had an intensity greater than 5% of the peak intensity in the original summed image maps; signal-to-noise at this contrast ratio was greater than 2.

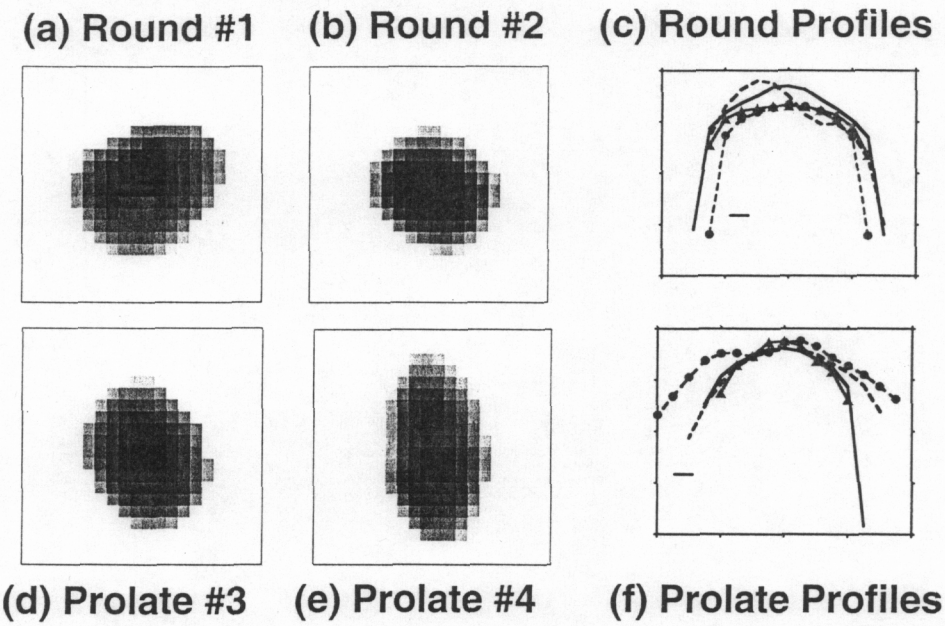

Figure 3: T_e maps and profiles from several experiments. In (a) and (b), the laser pointing was identical and tuned to produce a nearly spherical imploded core; in (d) and (e) the laser drive symmetry was tuned to produce prolate asymmetry. The scale for the images is 100 μm square at the source, and the vertical and horizontal profiles for the images are shown in (c) and (f). The hohlraum axis is vertical.

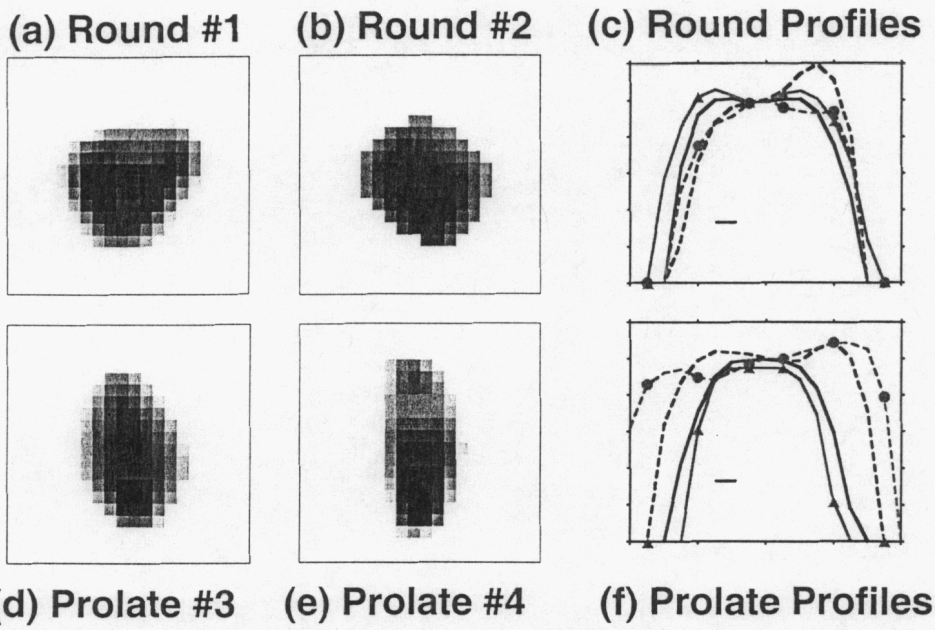

Figure 4: Scaled N_e maps and profiles. The cases are the same as shown in Fig. 3.

III. CONCLUSIONS

The two-lobed structure evident in the prolate-drive Te and Ne profiles is intriguing. As the drive becomes more prolate (equator-high), the compressed core appears to split, and exhibits peaks in both temperature and density. These features are invisible in broadband x-ray images at comparable energies, but have been observed in broadband ~ 9 keV x-ray images obtained from similar implosions. Furthermore, the data suggest that even slight prolate-drive asymmetry can produce this structure, as evident in Figs. 4(b) and 4(d). We also note that a shell-like density structure is evident when drive symmetry is good, as shown in Fig. 4(a). This is consistent with expectations based on hydrodynamics simulations and analytical predictions [1].

Future work will concentrate on obtaining time-gated data from similar implosions, and on two-dimensional hydrodynamics simulations to explore the nature of the two-lobed structure.

ACKNOWLEDGMENTS

This work was performed under the auspices of the U.S. Department of Energy by the University of California Lawrence Livermore National Laboratory under contract No. W-7405-ENG-48, and by the University of Nevada, Reno, under DOE NLUF Grant No. DE-FG03-03SF22696. Partial support was also provided by DoE HEDS Grant No. DE-FG03-98DP00213 to Howard University.

REFERENCES

[1] J. D. Lindl, *Inertial Confinement Fusion* (AIP Press/Springer-Verlag, New York, 1998).

[2] I. Golovkin *et al.*, Phys. Rev. Lett. **88**, 045002-1 (2002).

[3] I. Uschmann *et al.*, Appl. Opt. **39**, 5865 (2000).

[4] Laboratory for Laser Energetics, University of Rochester.

[5] B. Yaakobi *et al.*, Phys. Plasmas **7**, 3727 (2000).

[6] B. Yaakobi, F. J. Marshall, D. K. Bradley, Appl. Opt. **37**, 8074 (1998).

[7] K. Bockasten, J. Opt. Soc. Am. **51**, 943 (1961).

[8] I. E. Golovkin *et al.*, J. Quant. Spectrosc. Radiat. Transfer 65, 273 (2000).

[9] R. Turner, LLNL (personal communication).